ANALYSIS OF FAILED FORGING SADDLING MANDRELS AND PROCESS IMPROVEMENTS FOR INCREASED MANDREL LIFESPAN

Materials Engineering Department Senior Project

Brock Costalupes
Advisor: Prof. Blair London
Industry Sponsor: Schlosser Forge Co.
6/1/2012

Approval Page

Project Title: Analysis of Failed Forging Saddling Mandrels and Process Improvements for Increased Mandrel Lifespan

Author: Brock Costalupes

Date Submitted: June 1, 2012

CAL POLY STATE UNIVERSITY

Materials Engineering Department

Since this project is a result of a class assignment, it has been graded and accepted as fulfillment of the course requirements. Acceptance does not imply technical accuracy or reliability. Any use of the information in this report, including numerical data, is done at the risk of the user. These risks may include catastrophic failure of the device or infringement of patent or copyright laws. The students, faculty, and staff of Cal Poly State University, San Luis Obispo cannot be held liable for any misuse of the project.

Prof. Blair London _____

Faculty Advisor Signature

Prof. Trevor Harding _____

Department Chair Signature

Abstract

This project seeks to increase the lifespan of steel mandrels used by Schlosser Forge in the saddling process, which is part of the production of forged rings for the aerospace and power generation industries. All saddle mandrel samples were taken from used 4340 steel mandrels. Hardness profiles were measured across rectangular bars cut from the transverse direction of a completely fractured piece of a 7□ diameter mandrel. The hardness near one outer surface of the tested bar was 36 HRC and gradually decreased to 30.5 HRC at the opposite surface. Macroscopic examination of the primary fracture surface along with light microscope imaging of fracture surface feature details suggests that the failure mechanism is likely related to reversed bending fatigue rather than deterioration of the mechanical properties of the steel due to microstructural changes from in-process overtempering during saddling. Cyclic softening of the quenched and tempered steel caused by the saddling process adversely affects the ability of the steel to withstand fatigue. Different heat treatments were conducted to compare the resulting toughness, measured by Charpy impact test, to that of the current process of quenching and tempering the mandrel to a hardness of 38 – 42 HRC. Each heat treatment involved austenitizing at 1500°F for one hour. By varying the tempering temperature, with a constant two hour tempering time, samples were obtained at 28.5 HRC, 39.8 HRC, and 42.5 HRC. Charpy impact energy decreased significantly as hardness increased. An additional heat treatment was conducted where a 4340 steel sample was austenitized, quenched in a 660°F $NaNO_3$-based molten salt bath and held for two hours. The result of this heat treatment is a bainitic structure, which may show improved toughness.

Keywords: forging, materials engineering, saddling, 4340 steel, fatigue, austempered, ring rolling, bainite, superalloy

Table of Contents

List of Figures

List of Tables

Introduction

Seamless rings may seem trivial in name, but complex systems such as the turbines that power jet planes and produce energy at power generation plants would be unable to function without them. These rings are in fact the casings, shrouds, seals, gaskets, and spacers that form the superstructure of the powerful turbine engine. These rings can be manufactured from alloy steels, stainless steels, aluminum alloys, titanium, and nickel-based superalloys such as Waspaloy and IN718. Firth Rixson, based in the United Kingdom, is a world leader in aerospace manufacturing, and forged rings are their largest division. They have six ring forging facilities worldwide; one in the UK, one in China, and four in the United States. One of the US-based facilities is Schlosser Forge Co. (Rancho Cucamonga, CA), which is capable of supplying the largest seamless and contoured rings that Firth Rixson offers. Schlosser Forge has been an industry leader for over 30 years and serves the aerospace, power generation, defense, and space propulsion industries. They are equipped with six hydraulic presses ranging from 750 to 4000 tons, vertical ring mills, radial ring mills, sizers, and a shrinker in a 260,000 sq. ft. manufacturing facility[1].

Ring Rolling

Seamless rings are forged in a process known as ring rolling. The steps of the process are illustrated in Figure 1. Step (a) shows the initial metal stock, which has been cut to a certain size and rounded. The processing step being performed in (a) is called upsetting, which is a forging technique where the diameter of the workpiece is increased by compressing its length. In step (b), the workpiece is punched and pierced by the hydraulic press to form the hole in the center. Step (c) shows the workpiece after the initial forming stages; it is now called a ring preform. The different components are identified in (d), which is the first step in the ring rolling process. In this stage, the idler roll presses the wall of the preform into the drive roll. As shown in step (e), the pressure on the ring due to the relationship between the idler roll and drive roll increases the diameter of the ring as the wall thickness of the preform is reduced. This dimension is controlled by the axial rolls. The ring rolling process continues until the required dimensions have been attained, which can result in a significant increase in diameter of the ring

as seen in step (f). By changing the angle of the drive roll, the angle and diameter of the idler roll, and the angle and position of the axial rolls, rings of complex cross-section and various diameters can be forged.

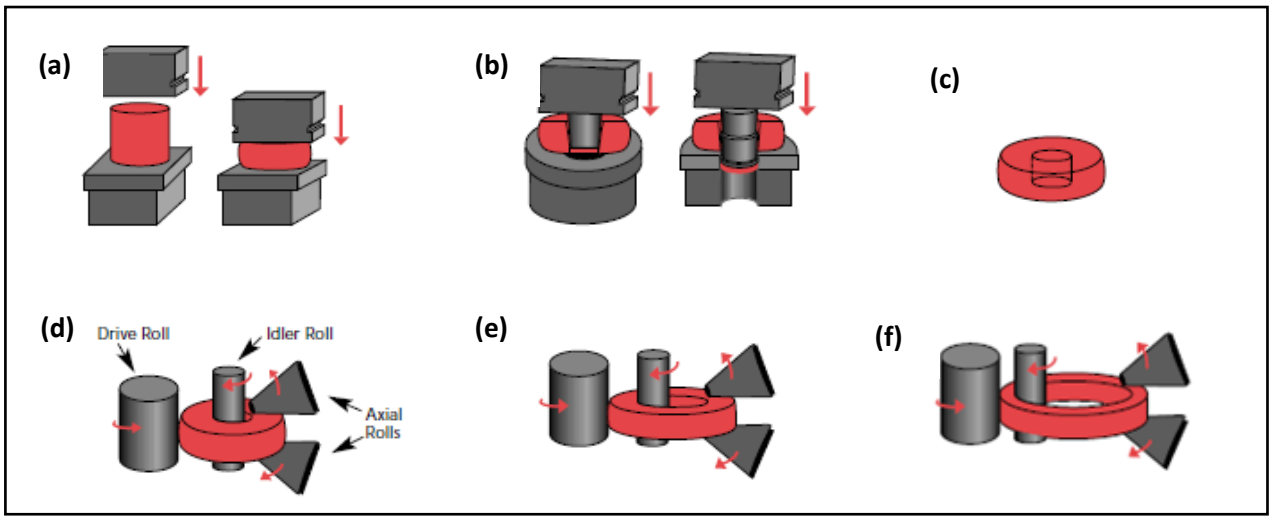

Figure 1: The schematic depicts the ring rolling process. The workpiece is in red, which is an accurate depiction as the alloy must be heated to a temperature above its recrystallization temperature for hot forging. The ring rolling process produces parts of greater quality compared to casting, machining, welding, or closed die forging[2].

The high temperature plastic deformation of the metal during forging results in several microstructural changes that result in rings of higher quality than those produced by other processing techniques. One important characteristic of forging is its effect on grain size and orientation. In a forged part, grain directionality can be controlled by the designer. This can be used to tailor the maximum strength of the part to be in the direction of its eventual maximum loading. Additionally, the grains will flow along with the contours of the part, unlike in a machined part which will expose grain ends and negatively affect the final part. In cast parts, the grains lack a common directionality and a large grain size distribution is present throughout the part. Also, the high pressures inherent in forging eliminate porosity in the cast alloy and also eliminate the remnant dendritic structure of the original ingot[2]. Welded parts have inconsistent properties along the weld, and heat affected zones present problems like reversal of strengthening mechanisms and increased corrosive attack.

Saddling

For relatively large diameter rings, additional processing steps are required before a preform is ready for the ring rolling process. One such processing step employed at Schlosser Forge is called “saddling”. The goal of this step is to increase the inner diameter of a ring forging preform. Figure 2 depicts the main points of the saddling process, in which a steel mandrel is held at one end and a hot preform is placed around the mandrel. A typical mandrel is 7-9□ in diameter and 120□ long, at a weight of about 1,300 pounds. In this stage of processing, the alloy preform is heated well above its solutionizing temperature so that it is as malleable as possible; the exact temperature varies greatly with alloy, but it is typical for the mandrel to experience a workpiece heated to around 2,000°F. The mandrel, and thus the preform, is rotated and the preform is struck by an upper die. The surface finish, dimensional tolerances, and resulting material properties are of secondary importance because these specifications are met in subsequent forging and heat treatment stages.

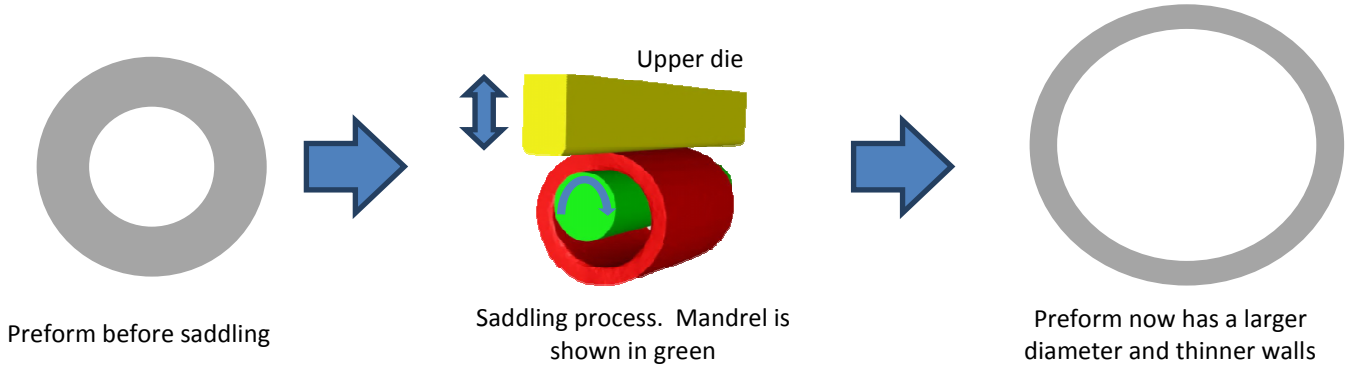

Figure 2: The saddling process typically begins with a preform that has a diameter 0.5 inch larger than the mandrel and ends with a ring that is large enough for the desired ring rolling operation.

Problem Statement

The saddling process imparts great forces onto the workpiece and the mandrel and a large amount of heat transfer occurs from the hot preform to the 4340 steel mandrel. Also, during the saddling operation the mandrel in bending as it is being loaded by the upper die; this adds fatigue to the mandrel, which is already experiencing dynamic loading at high stress and thermal fluctuations. These conditions lead to frequent fracture of saddling mandrels and thus

the need to constantly replace the mandrels. The fractured mandrels are not only an issue when it comes to cost, but also to workplace safety as the stresses involved in fracturing such large pieces of steel are high. The purpose of this study is to identify the mechanisms involved in the fracture of a 4340 steel saddling mandrel and to establish a heat treatment method that optimizes the lifetime of future mandrels.

4340 Steel

AISI/SAE 4340 steel is a common Ni-Cr-Mo low alloy steel. It is typically used for such applications as bolts, screws, gears, pinions, shafts, crankshafts and piston rods for engines, aircraft landing gear, and various structural pieces in aircraft. The composition range for 4340 steel is shown in Table I.

Table I: Chemical composition of 4340 steel.

Composition Range for 4340 Steel								
Element	C	Cr	Mn	Mo	Ni	P	S	Si
Weight %	0.41	0.8	0.7	0.25	1.8	0.02	0.02	0.25

Table II shows typical mechanical property values for 4340 steel that has been oil quenched and tempered at 425°C, which is comparable to the heat treatment performed on the mandrel sample supplied for this study.

Table II: Property values of 4340 steel[3].

Mechanical Properties of 4340 Steel	
Elastic modulus	30,300 ksi
Flexural modulus	30,300 ksi
Yield strength	198 ksi
Tensile strength	213 ksi
Compressive strength	198 ksi
Elongation	10% strain
Fracture toughness	77.4 ksi in^0.5
Fatigue strength at 10^7 cycles	81.2 ksi

There are multiple reasons why this particular alloy is chosen for the saddling process. 4340 steel is considered the standard by which other high-strength steels are compared. It has high hardenability, ductility, toughness, strength, creep resistance, and fatigue strength. Another attribute that makes this steel a good choice for saddling is that it is nearly immune to temper embrittlement, which can significantly decrease the toughness of low-alloy steels slowly cooled through the temperature range of 300 – 600°C[4]. However, as impressive as its mechanical properties are, the primary reason this material is chosen for saddling is because it is strong enough to do the job and inexpensive enough that replacing a broken mandrel can be written off as a standard operating cost. The Cambridge Engineering Selector software lists the cost of 4340 steel as ranging between 0.561 – 0.617 $/lb.

Steel Microstructure

The properties of a steel sample can be directly attributed to its microstructure. In steel the primary constituents of the microstructure are ferrite and cementite at room temperature, and austenite at elevated temperatures. Ferrite is a solid solution, meaning that the iron maintains a body centered cubic crystal structure, but contains an amount of carbon (maximum of 0.022%) in solution in interstitial sites based on the temperature of the steel. Cementite, Fe_3C, is an intermetallic compound of Fe – 6.67 wt% C. Iron and Fe_3C form the boundaries for the iron-carbon phase diagram (Figure 3), which gives the best idea of what phases to expect at different compositions and temperatures. At 0.77% C is the eutectoid composition.

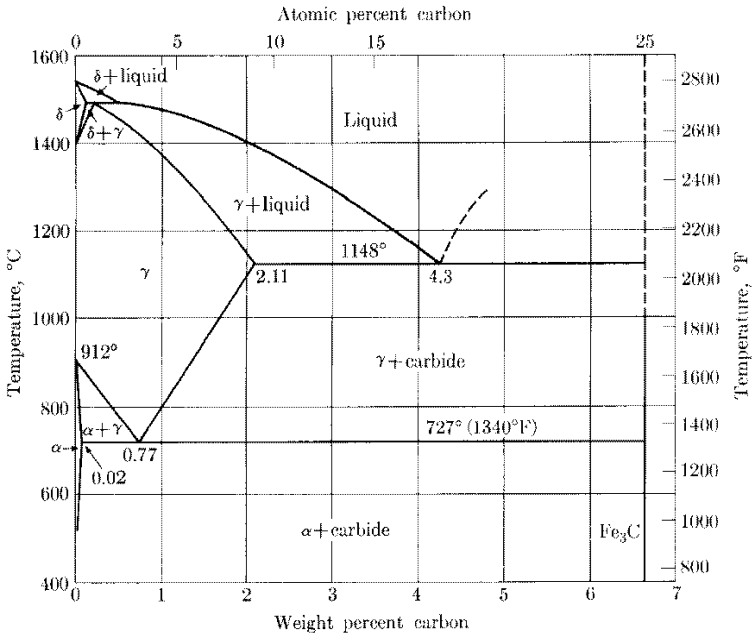

Figure 3: Phase diagrams are an equilibrium construction, so are only applicable when cooling the alloy slowly. Also, the Fe-C phase diagram does not account for additional alloying elements, as are present in 4340 steel[5].

At this point on the diagram as austenite (which is a face centered cubic phase in steel that only exists above the eutectoid temperature) is cooled below the eutectoid temperature (727°C) there is sufficient thermal driving force to cause the austenite to decompose into ferrite and cementite. This causes the growth of pearlite, which is a lamellar microstructural constituent consisting of plates of Fe_3C in a matrix of ferrite. Since the austenite phase previously held all of the carbon in the steel, it must reject all of the carbon that is not able to dissolve in the ferrite. This causes the bands of cementite as carbon diffuses out of the ferrite and forms Fe_3C bonds.

Since 4340 is not a plain carbon steel, there are effects that alloying elements cause in the formation of pearlite that do not appear on the phase diagram. Nickel and manganese tend to decrease the eutectoid temperature by making the austenite phase more stable, while elements like silicon, chromium, and molybdenum increase the eutectoid temperature. As shown in Table I, eutectoid temperature decreasing elements are present in amounts twice as much as those elements that increase the eutectoid temperature. Another effect caused by most alloying elements in steel is to decrease the rate at which pearlite forms. This occurs because when elements such as Ni and Si are dissolved in austenite it is energetically favorable for them to remain in solution. This means that the alloying elements must diffuse away from the cementite as it grows, and they do this slowly because unlike carbon they are substitutionally dissolved[6]. In 4340 steel the effect of the presence of all of the aforementioned alloying elements creates a separation of the proeutectoid ferrite and pearlite formation from the range of bainite formation, as seen in the isothermal transformation (IT) diagram in Figure 4.

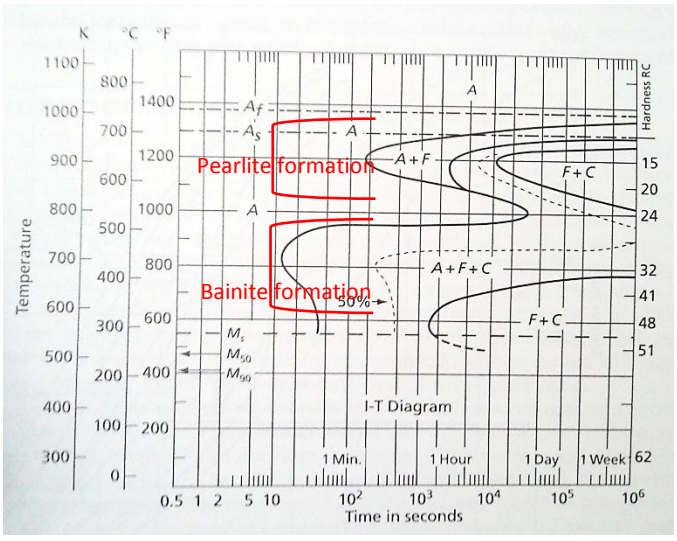

Figure 4: IT diagram for 4340 steel. The "bay" in between the pearlite (upper) and bainite (lower) noses is a region where austenite remains stable as the dissolved atoms take more time to diffuse out of solution due to a lack of thermal energy to form pearlite and insufficient undercooling to form bainite[7].

Proeutectoid ferrite is a phase that forms in hypoeutectoid steels as austenite decomposes as it cools (Figure 5). In Figure 3, any steel with a composition less than the eutectoid composition of 0.77% carbon is a hypoeutectoid steel. Upon cooling, as the temperature passes through the range containing ferrite (α) and austenite (γ), the ferrite that forms as γ decomposes and becomes more carbon rich is a stable phase and will remain as the steel cools to room temperature. This results in a microstructure of pearlite and proeutectoid ferrite formed around the pearlite grains. 4340 steel is a hypoeutectoid alloy, which is the cause of the A + F region in Figure 4. It is important to note that only the austenite is capable of transforming into pearlite, bainite and martensite.

Figure 5: Proeutectoid ferrite formation upon cooling from austenite. From left to right: ferrite nucleates at the grain boundaries, increases in volume, and then as the steel traverses the eutectoid point pearlite forms (dark gray)[8].

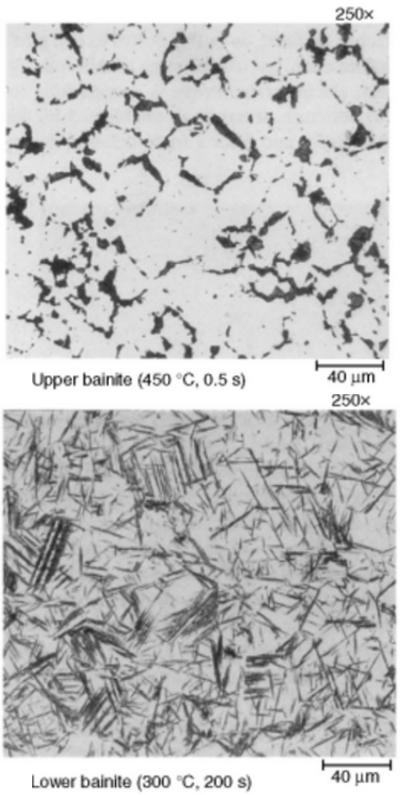

Figure 6: Lower bainite is formed at lower temperatures than upper bainite and has a distinctively needle-like appearance. In both micrographs the dark areas are cementite and the light is ferrite[9].

Bainite is a microstructural constituent formed through a mix of diffusion and shear. Bainite occurs under conditions of sufficient undercooling, yet still allows carbon to diffuse out of austenite, and consists of ferrite and cementite. Instead of a lamellar structure as in pearlite the cementite forms in needle-like configurations (Figure 6). Lattice shear and diffusion are the mechanisms of bainite formation. Because it has a finer structure than pearlite, bainite is typically harder and tougher than pearlite.

Perhaps the most important phase for the steel saddle mandrels is martensite. The martensite transformation does not rely on diffusion and is instead dependent only on the cooling rate of austenite, which is the only phase from which it can be formed. Martensite has a body centered tetragonal

(BCT) crystal structure that occurs when the iron atoms of the FCC crystal structure of austenite shear along {111} planes. As the FCC austenite becomes unstable during cooling, it attempts to transform into BCC ferrite as it would during slow cooling; however, the interstitial carbon atoms that are unable to diffuse out of the austenite due to a lack of thermal driving force place a lattice strain on the austenite. Under a fast enough cooling rate, the strain is overcome and the iron atoms shift by approximately an interatomic spacing. The resulting BCT structure is less densely packed than BCC and thus results in a volumetric expansion and hardening of the steel. The transformation occurs within the steel at roughly the speed of sound[9]. The martensite microstructure in steel assumes either of two forms depending on the carbon concentration of the steel; plate martensite in high carbon steel or lath martensite in lower carbon steels (typically below 0.6%). For 4340 steel we can expect to find a microstructure consisting of lath martensite (Figure 7) upon sufficiently rapid cooling. Martensite is an extremely strong phase in steel, but with its strength it loses the ability to plastically deform and is simultaneously extremely brittle. However, it is a supersaturated solid solution of carbon in iron so by adding thermal energy to the system the steel will decompose into more stable constituents through the process of diffusion (tempered martensite).

Figure 7: This micrograph is a mix of plate and lath martensite at 1000x magnification[10].

Tempering

Martensite is the strongest phase in which steel can exist; however, its almost total lack of ductility renders it virtually to useless in engineering components. After austenitizing the steel and quenching it to form martensite, the steel can be reheated to a temperature below the eutectoid temperature for an amount of time based on the size and thickness of the part; this is called tempering. Since martensite is a supersaturated solid solution, the thermal energy provided during tempering allows the carbon and alloying elements to diffuse out of the martensite. If the steel was cooled fast enough to transform all of the high-temperature

austenite to martensite, the resulting microstructure will not contain any proeutectoid ferrite, pearlite, or bainite formed during cooling; where the martensite used to be, a fine distribution of carbides in a ferrite matrix will be found. This microstructural constituent is called tempered martensite (Figure 8). This transformation reduces the strength and hardness inherent in martensite, but restores some toughness and ductility (Figure 9).

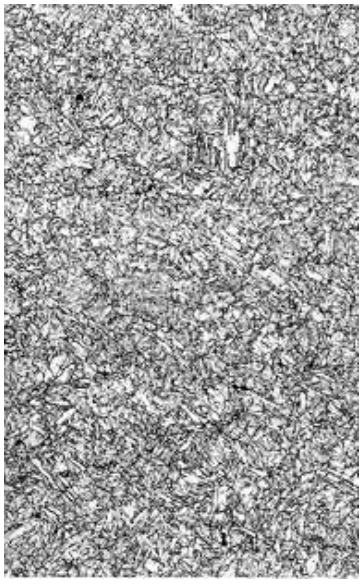

Figure 8: The fine structure of tempered martensite is what lends it its desirable mechanical properties[11].

There are several mechanisms present in during the tempering of martensite. At low temperatures during the tempering process, the carbon atoms are segregated to lattice defects in the material like dislocations. Carbon atoms also cluster during tempering and eventually lead to the precipitation of carbides, most notably epsilon carbide which has an HCP crystal structure. Also, during tempering any retained austenite decomposes into a bainitic constituent. At higher tempering temperatures the carbides and segregated carbon become rod-shaped cementite particles. In the matrix, recovery and recrystallization of the ferrite structure occurs[8]. Alloying elements also play a role in how the martensite responds under tempering. Si and Ni inhibit the growth of carbides because they are partitioned to ferrite and must substitutionally diffuse out of the way making it more difficult for the carbon to cluster into carbides such as cementite. Mn can result in finer ferrite grains by impeding the movement of the boundaries between ferrite grains by introducing solute drag. Solute drag is an effect that is due to alloyed solute atoms to segregate at or away from intercrystalline boundaries. The segregation of these solute atoms lowers the surface energy of the grains and removes some of the driving force for grain growth[6]. In low alloy steels such

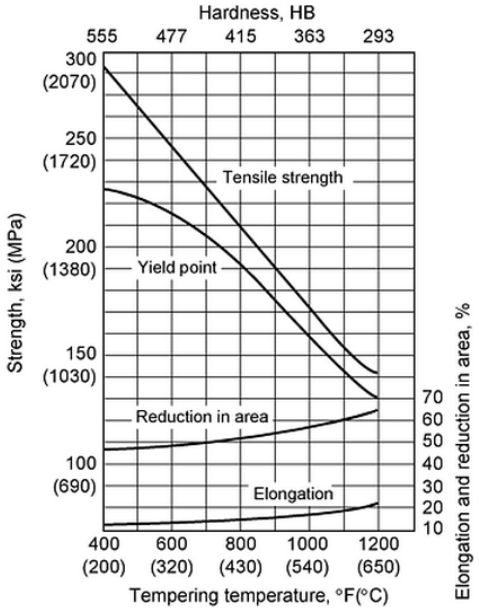

Figure 9: Tempering temperature has an effect on all of the mechanical properties of steel. This diagram shows a linear trend between the tensile strength and tempering temperature of 4340 steel[10].

as 4340, high tempering temperatures result in alloying elements forming their own carbides in a fine distribution of precipitates. These carbides form at high temperature because the growth rate of the carbides is based on the diffusion rates of the solute atoms through ferrite. This makes up for the softening of the steel at lower tempering temperatures due to the Ostwald ripening of cementite precipitates.

An important parameter when tempering martensitic steel is the temperature at which the steel is reheated. Lower temperatures do not provide enough driving force to make the alloying elements diffuse through the iron matrix, high tempering temperatures exponentially increase the rate of diffusion and the resulting microstructure can develop spheroidized cementite. Spheroidized cementite is formed during long periods of Ostwald ripening, where larger cementite precipitates grow at the expense of smaller precipitates. This results in large distances in the ferrite matrix between large cementite particles and thus soft, weak steel.

Fatigue Fracture

Fatigue fracture occurs under cyclic or repetitive loading and can happen when the applied stresses are below the yield strength of the material. A fatigue fracture usually occurs in three stages: I) initiation of a crack, II) propagation of the crack through most of the length of the fracture, and III) final propagation of the crack and thus complete failure.

In fatigue crack initiation, or stage I fatigue, the microstructure, mechanical properties, and the mean stress are highly influential. A stage I crack typically follows crystallographic planes, but can change directions at discontinuities. A fatigue crack is initiated at anything that can cause a localized stress concentration at the surface of the metal, such as an inclusion, corrosion pit, or scratch. The mechanism behind stage I fatigue is principally slip-plane cracking due to repetitive reversals of the active slip systems in the metal[12]. Up to 90% of the fatigue life of a material can be initiating a viable crack in stage I.

Stage II fatigue represents the largest portion of fatigue fracture. This fatigue stage is not as dependent upon the microstructure and mechanical properties of the metal as stage I fatigue and is instead highly dependent upon the amplitude of the alternating stress. Defining

marks of stage II fatigue are fatigue striations at the microscopic level, and beach marks at the macroscopic level. Both marks signify periods of loading and unloading. Stage II cracks typically occur as transgranular fracture and may propagate as illustrated in Figure 10. Stress concentrated at a fatigue crack results in plastic deformation at a small region at the crack tip, while the rest of the material still experiences only elastic strain. Under the tension portion of the load cycle, the crack tip opens through slip on alternating slip planes. Eventually, the crack tip blunts and restricts the crack from progressing; however, as the load declines due to the opposite portion of the loading cycle, the crack tip is resharpened by partial slip reversal. This results in compressive stress at the crack tip due to the relaxation of the residual elastic tensile stresses induced in the surrounding, uncracked material during the subsequent rising portion of the load cycle, thus advancing the crack[12].

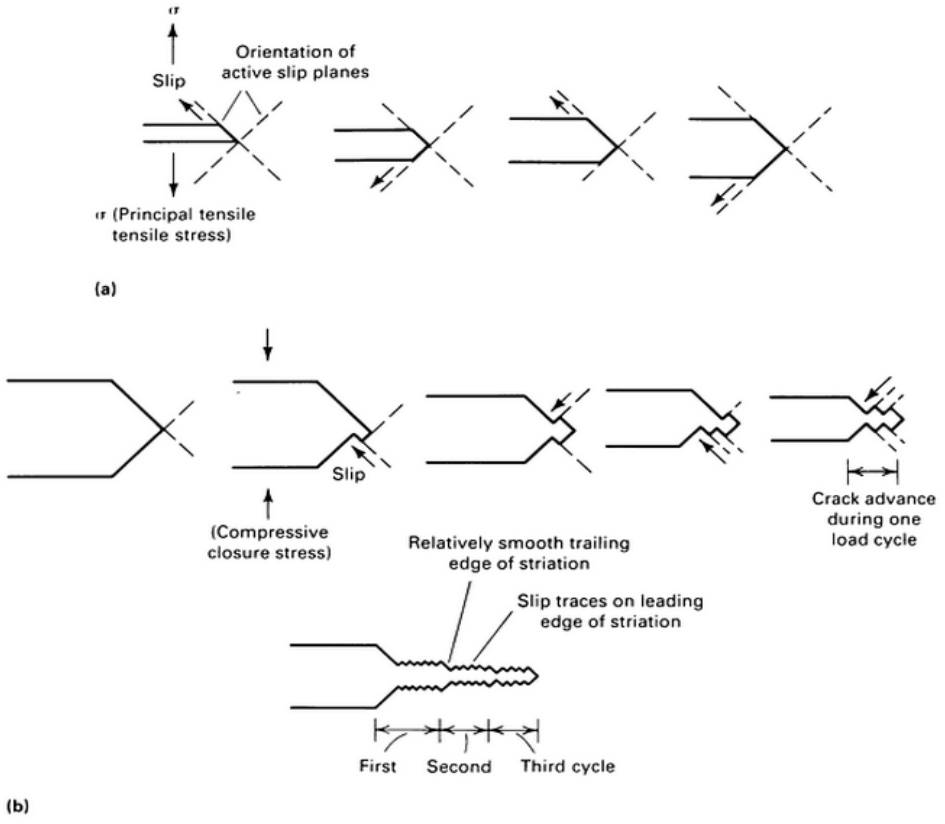

Figure 10: Mechanism of fatigue crack propagation by alternating slip at the crack tip. (a) Crack opening and crack tip blunting by slip on alternate slip planes with increasing tensile stress. (b) Crack closure and crack tip resharpening by partial slip reversal on alternate slip planes with increasing compressive stress[12].

Stage III fatigue is overload or tensile fracture, but the cross sectional area has been drastically reduced due to the large stage II cracking. Stage III thus exhibits characteristics of dimple rupture.

Realistic Constraints[13]

This project deals with the behavior of large steel mandrels under conditions of high temperature, repeated thermal loading, and cyclic loading of high stresses. The data for this project is based on small samples taken from these mandrels. It is not within realistic economic constraints to run experiments using entire 4340 steel mandrels as samples. According to the Cambridge Engineering Selector software, the price of quenched and tempered 4340 steel is approximately 0.59 USD/lb.[3] A 7□ diameter mandrel under this cost estimate is valued at $880, not to mention the costs associated with shipping, labor used during tests, and downtime of the saddling equipment. Under these economic constraints it is not possible to evaluate the effectiveness of a heat treatment or other processing step recommended in this study on mandrels under actual saddling conditions because a failed test would cost the company money in materials and production time. However, it is within the scope of the broader impacts of this study to decrease the accumulation of the new mandrel costs introduced above by increasing the lifespan of each mandrel, leading to savings for Schlosser Forge.

This study also aims to improve upon the health and safety conditions associated with the saddling process. As a mandrel weakens with repeated use, it becomes more susceptible to fracture. Since these mandrels are under such extreme stress and thermal conditions, when they fracture they do so with violence and may send pieces of steel outward at dangerous velocity. According to a report by the Bureau of Labor Statistics on workplace injuries and illnesses for 2010, the number of recordable workplace injuries in the fabricated metal product manufacturing industry was 68,800 cases. This is a rate of 5 workers per every 100 workers[14]. It is a goal of this project to help ensure that the rate of injury at Schlosser Forge is well below this national average.

Experimental Procedure

Several samples were taken from used 4340 steel mandrels at the Schlosser Forge facility. The samples were cut by a large band saw from either 7″ or 8″ diameter mandrels. A total of five mandrel slices, shown in Figure 11, varying in thickness from 2.5″ to 4″ were prepared. The five samples covered the following mandrel conditions: complete fracture of a 7″ diameter mandrel, mid-mandrel sample of an 8″ diameter mandrel, a section of an 8″ mandrel containing initial cracking, and a piece from the end of both an 8″ and a 7″ mandrel. All of the sample sections were confirmed to be 4340 steel through use of a portable x-ray fluorescence spectrometer. Due to the high hardness of 38 – 42 HRC and the large diameter-to-thickness ratio of the sample disks, locating a machine shop capable of dividing the disks into smaller samples was difficult because it was not possible for a band saw to grip the disk. Ultimately, smaller samples were cut from the disks by a water jet cutter. The water jet only allowed cuts from the face of the disks, meaning that it was not possible to slice disks of lesser thickness from the main disk. As a result, all subsequent hardness testing and metallographic analysis were performed from samples cut from rectangular bars obtained in the manner illustrated in Figure 12.

Figure 11: The five mandrel samples provided a total of 220 pounds of steel for further analysis. Fracture surface of a mandrel is in the center.

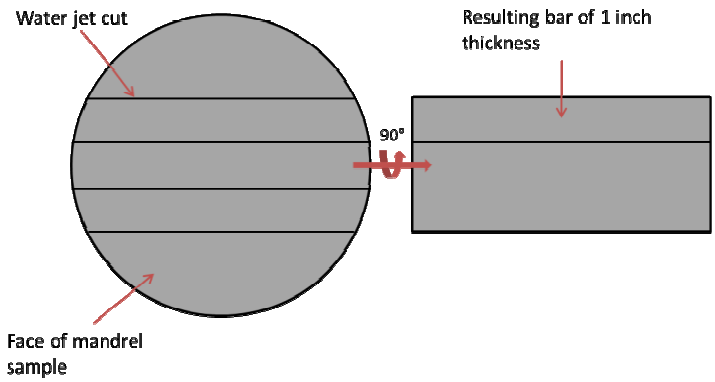

Figure 12: This illustration shows the cutting plan used for obtaining thinner sections of the initial mandrel samples. Using this technique, the resulting pieces included one 1 inch thick bar that spanned the full diameter of the mandrel, and two additional one inch thick bars.

Hardness Profiles

Hardness profiles were measured for both the end piece of a 7□ diameter mandrel and the fully fractured mandrel sample. All hardness measurements were taken in the Rockwell C scale with a diamond indenter, following ASTM standard E18-11[15]. The goal was to measure hardness as a function of distance from the exterior surface of the mandrel to investigate possible overtempering of the mandrel surface, or near surface. For the end piece sample, the bar tested was a diameter-spanning bar obtained as illustrated in Figure 12. Due to the arm on which the nozzle for the water jet was mounted interfering with the jagged peaks of the fracture surface, it was not possible to obtain diameter-spanning sections from the fractured mandrel sample. The actual rectangular sections were cut from a chord at a maximum of approximately 1.2□ from the mandrel surface. The sections were 1/2□ in thickness and the hardness profiles were measured on the transverse faces, as shown in Figure 13. The hardness profiles for the end piece bar were measured on the face parallel to the flat face of the original disk.

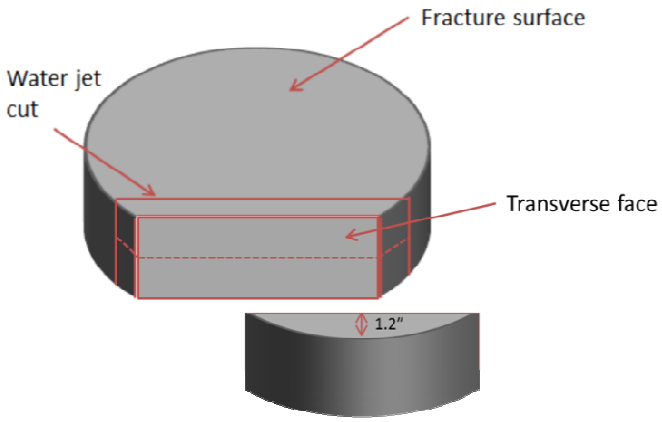

Figure 13: This cutting scheme illustration shows the resulting two sections (denoted by the solid and dotted red lines) that were used as hardness profile specimens. The labelled transverse face is where the hardness measurements were done.

The 4340 steel disks were thick enough and hard enough that as the water jet reached a certain thickness during cutting, the edges of the cut slightly deflected the jet, resulting in grooves in some of the faces of the hardness profile sections. To remove the grooves, the surfaces were ground with an angle grinder equipped with a grinding wheel followed by an 80 grit finishing wheel. Each hardness indentation does not have its own dimensional coordinates; instead, for each rectangular section there are a series of zones that each contain from five to twelve hardness measurements. The zoning method for both types of mandrel samples are shown in Figure 14. Hardness measurements were taken sequentially, zone by zone.

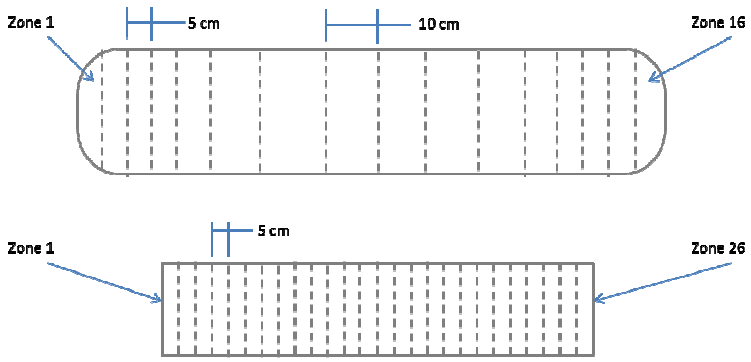

Figure 14: At the top is the zoning diagram for the end piece hardness profiles, the bottom diagram is the zoning scheme for the fractured mandrel hardness profiles. The zoning method eliminates the need to measure the location of each indentation.

Metallography

In order to provide information regarding the microstructure of the mandrel steel, metallography was conducted on the following samples: near the surface of an end piece, the interior of the same end piece, an area of the fractured mandrel sample that meets the original hardness specification, a softened area of the fractured mandrel, a section of mandrel steel quenched and tempered at 700°F, and a secondary crack cross-section. All specimens were cut from initial water jet sections by an abrasive cut-off saw (Leica MSX-250A) at around 3200 RPM with a 0.062□ thick blade. Most of the samples were mounted in a mineral filled diallyl phthalate thermoset mount with a hydraulic mounting press (Buehler SimpliMet 2). The two end piece sections were large enough that they did not need to be mounted for polishing.

After each sample was cut and mounted, they were ground and polished. The grinding process involved a series of grit sizes of 240, 320, 400, and 600. After each successive grit size, the specimen was cleaned and viewed under an optical lens at 50-100x magnification in order to ensure that all scratches from the previous, larger, grit were no longer present. After grinding at 600 grit, the samples were polished on rotating microfiber pads coated in first a 6 µm diamond suspension, and then a 1 µm diamond suspension. After a sufficient level of polish was obtained, the samples were etched for 15-30 seconds (depending on best results) with a 2% nital solution. The 2% nital etchant was mixed in batches of 25 mL containing 24.5 mL ethanol and 0.5 mL concentrated nitric acid. The best results were obtained by pouring a

quarter inch of etchant into a petri dish and holding the sample face-down for the specified time period. After etching, the samples were viewed with an inverted stage optical microscope (Leica DM IRM) at magnifications up to 1000x.

Heat Treatment

Four different heat treatments were performed on 4340 steel from the 8″ diameter end piece disk. Three samples, each approximately 3″ x 2.45″ x 1″, were removed from a larger section using the same abrasive cut-off saw used during preparation of the metallography samples. Heat treatments were performed successively, so that there was only one sample in the furnace at the same time. Each rectangular bar was austenitized in air at 1500°F for one hour in a Fisher Scientific Isotemp Muffle Furnace. In the furnace, the bars were placed on two alumina spacing beams so that the bottom side would not be too insulated. Furnace temperature was monitored via thermocouple during the heat up stage for the first austenitizing heat treatment and was found to be within +/- 3°F from the target temperature. The austenitizing temperature was the same as was listed on the heat treatment certification from Certified Steel Treating Corp. After the one hour austenitizing step, the bar was removed from the furnace and quenched in oil. The sample was agitated while cooling and remained in the oil bath for no less than five minutes. The next day, the martensitic bars were tempered in the same furnace for two hours at the following temperatures:

1. 1202°F to obtain 28-30 HRC
2. 842°F to obtain 38-42 HRC
3. 600°F to obtain 48 HRC

Upon removal from the furnace, the bars were placed on refractory bricks and allowed to cool to room temperature in still air. Each sample was labeled and tested for hardness at the surface using the Rockwell C scale with at least five tests at random locations on the bar.

The fourth heat treatment involved quenching austenitized samples and in a 660°F sodium nitrate/potassium nitrate molten salt bath with a two hour dwell time. Four samples were prepared using the abrasive cut-off saw, at dimensions of approximately 2.5 in x 0.7 in x 0.5 in. The heat treatment was carried out by Edward's Heat Treating Service (San Leandro,

CA). The resulting heat treated samples, along with those produced from the quench and temper heat treatments were packaged and sent to Dickson Testing for Charpy impact testing. The Charpy tests were performed according to ASTM standard E23-07a[16].

Fracture Analysis

The fractured mandrel sample was photographed with a 5 megapixel digital camera without magnification. A section was removed from the mandrel sample showing initial cracking such that multiple cracks were removed with the section. Using the abrasive saw, the section was cut at the edges of the visible crack. The remaining sample was secured in a vise and the crack separated by striking the portion above the crack with a hammer until the remaining cross section of the steel fractured, resulting in two pieces that each contained a fracture surface from the crack (Figure 15).

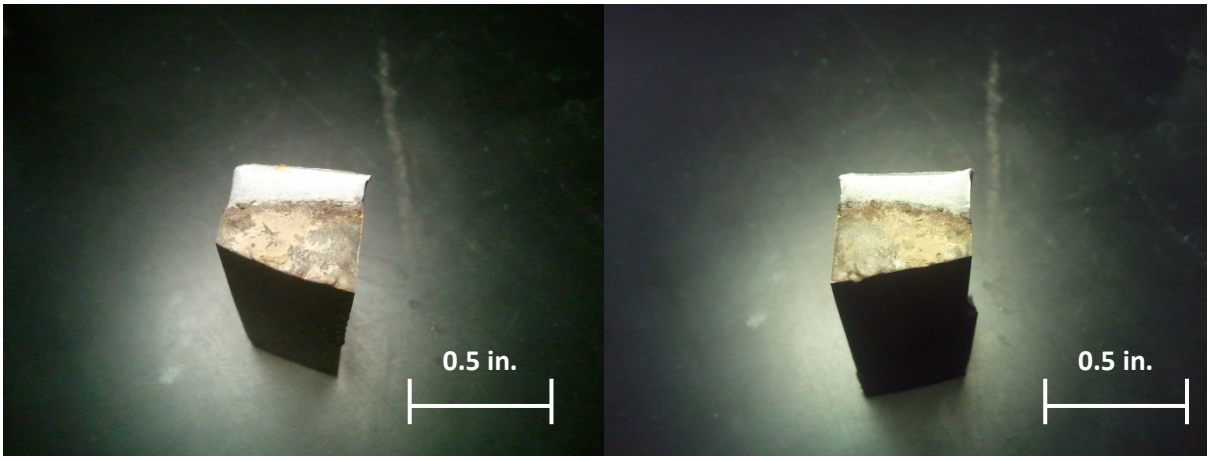

Figure 15: The darker, oxidized areas are the fracture surface from the saddling process. The bright gray areas were formed as the sample was fractured from hammer impact.

The brown material seen in Figure 15 was removed by using cellulose replicating tape by saturating the tape with acetone until gummy, adhering the tape to the sample, and after fully dry removing the tape. After the replicating tape procedure, the brown oxide and foreign material were completely removed. The fracture surfaces were then viewed under the SEM in high voltage mode with an accelerating voltage of 20 kV. Unfortunately, due to a strongly adherent high temperature oxide, useful SEM images were not obtained.

Results

Hardness Profiles

Figure 16 depicts hardness measurements from across the diameter of the unused mandrel end piece. Even at its hardest point, this section of the mandrel is still considerably softer than the specified hardness value of 38-42 HRC.

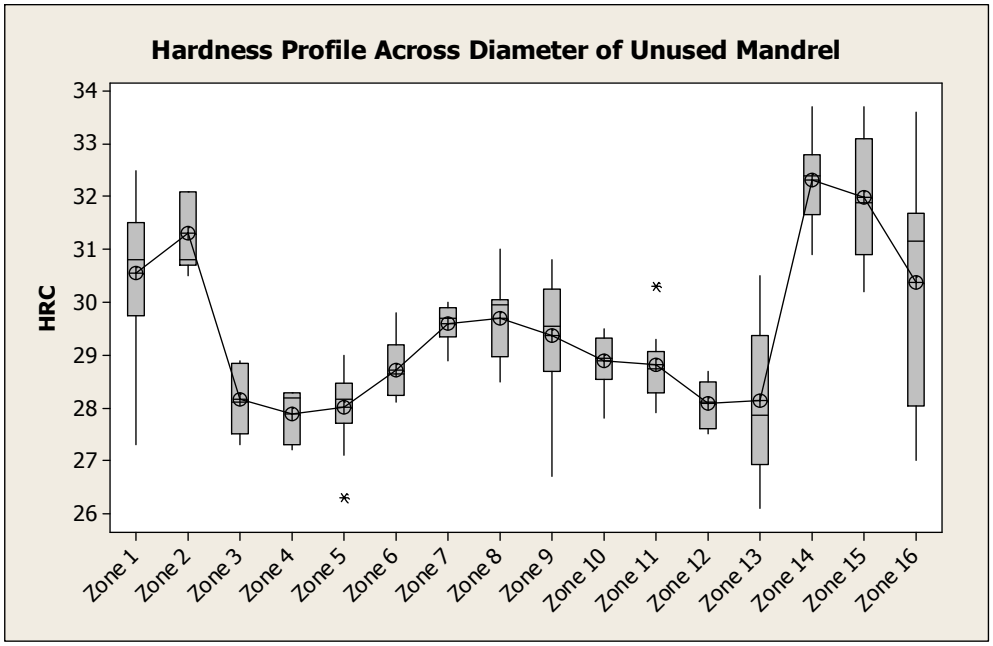

Figure 16: This representation of the hardness data for the unused mandrel shows a profile of hardness versus location while also providing an idea of the deviation of the data.

This high discrepancy in hardness in a section of the mandrel was not near the preform during the saddling process is most likely due to overtempering as the large mandrel was originally tempered for eight hours at 850°F. Because of the low hardness throughout the sample, this sample was not used as a control as was originally intended.

Figures 17 and 18 are both hardness profiles from the fractured mandrel sample. The profile in Figure 17 is from nearer the fracture surface than the hardness measurements in Figure 18. It is apparent in both graphs that the hardness decreases from the right side of the graph to the left side. The left side of the graph corresponds to the identified origin of the fracture that eventually led to the mandrel's failure. This means that mandrel failure may be facilitated by a softening of the steel near the surface of the mandrel.

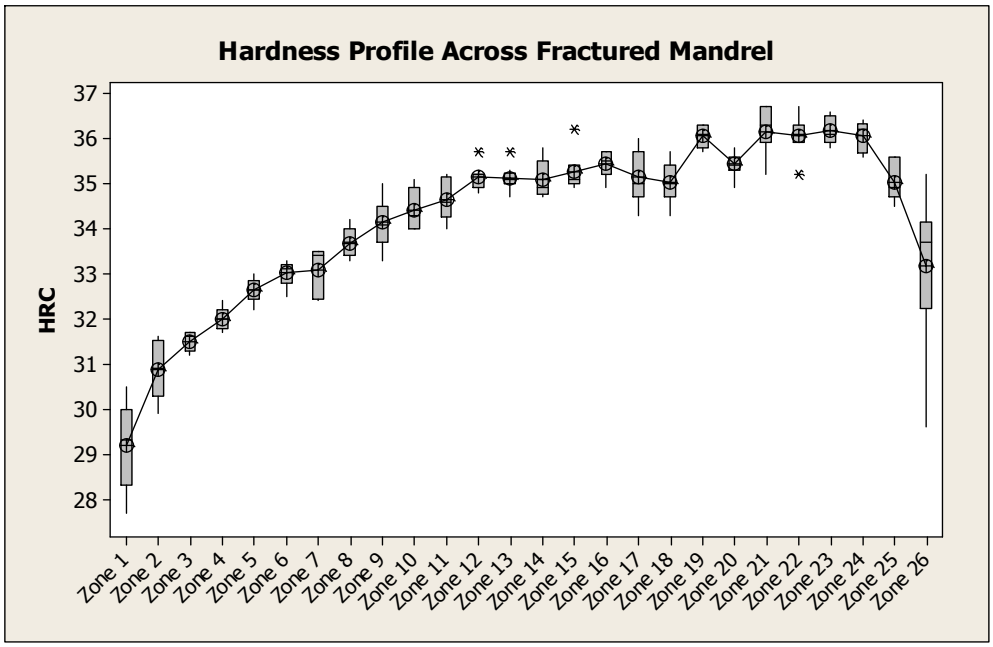

Figure 17: Since the mandrel rotates and the workpiece does not necessarily contact each point of the circumference of the mandrel evenly, hardness may be different at multiple points around the mandrel.

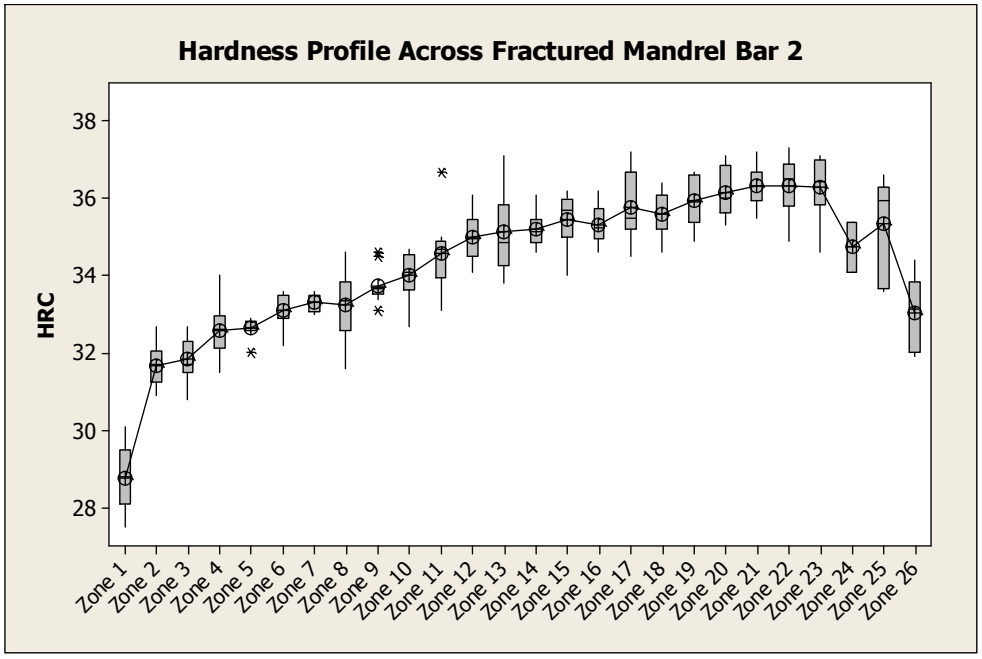

Figure 18: This hardness profile is slightly but uniformly harder than that of the sample measured in Figure 17, suggesting that the overall hardness slightly decreases over the 2-3 inches adjacent to the fracture surface.

The softening seems to occur relatively uniformly across the area of the mandrel underneath the preform. When the hardness was plotted as a function of distance from the fracture surface (parallel to the axis of the mandrel), there was no trend in hardness.

The software simulation pictured in Figure 19 is from the Forge 2011 software suite and models the heat transfer from an IN718 preform at 1800°F to the 4340 steel mandrel, which has been preheated to a temperature of 500 °F. Figure 19 depicts the maximum temperature reached during the saddling process.

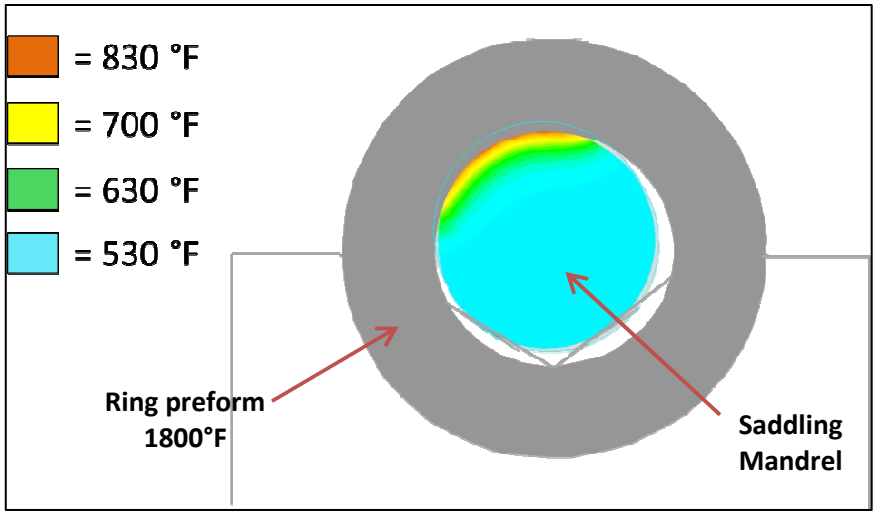

Figure 19: This cross section from a thermal simulation software model represents the location on the mandrel directly underneath the load. The temperature is not modeled in the preform. Also, the mandrel does rotate in the actual process, but due to functional limitations of the software program the preform rotates and the mandrel

The temperatures reached within the mandrel are within those used to temper 4340 steel; however, the saddling process only takes a few minutes until completion and is followed by water cooling the mandrels, so the time that the mandrel spends at elevated temperatures is too short to allow for significant diffusion-based softening of the steel during a single saddling operation. Overtempering may have an effect on mandrels that last through a large amount of saddling procedures. Alternatively, quenched and tempered steel is vulnerable to the phenomena of cyclic softening. The severity of the martensite quench traps dislocations in the metal, and even after tempering some of the dislocations remain. Upon cyclic strain of the

steel, the dislocations are freed and the net dislocation density decreases; this leads to the steel being softened[17].

Metallography

Because of the fine nature of the microstructural and hardening phases in tempered martensite, it is not possible to discern differences in the microstructure at the maximum available optical magnification of 1000x. Figure 20 shows a micrograph of the hardest segment of the sample measured in Figure 17 and Figure 21 is a micrograph of the softest segment. The differences in color are due to slight variations in etching time.

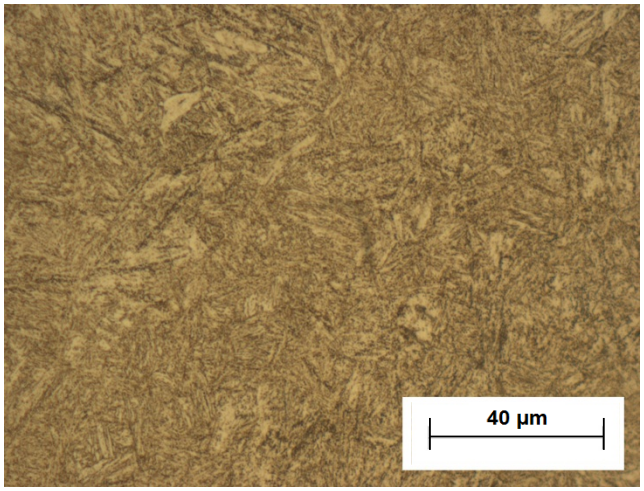

Figure 20: Tempered martensite nearly at the hardness specification of 38 HRC. This image was taken at 1000x magnification. Etched for 20 s. in 2% nital.

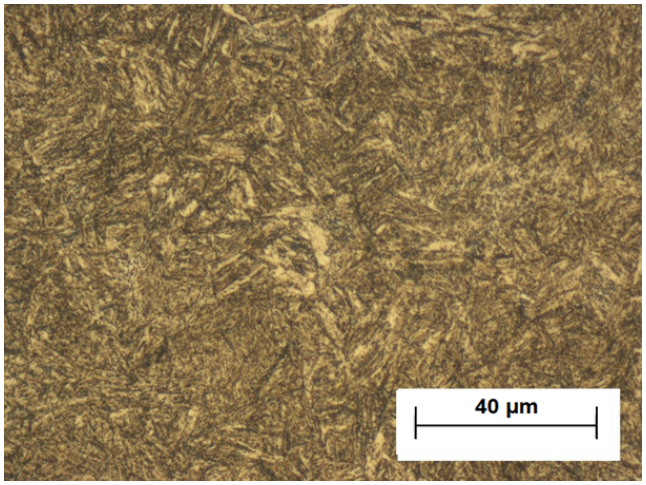

Figure 21: Tempered martensite nearly at approximately 31 HRC. This image was taken at 1000x magnification. Etched for 20 s. in 2% nital.

Fracture Analysis

The fracture surface in Figure 22 contains evidence of fatigue fracture. Since the mandrels are not plastically deformed with each loading cycle from the upper die, the stresses in the mandrel must not be in excess of the yield strength of 4340 steel.

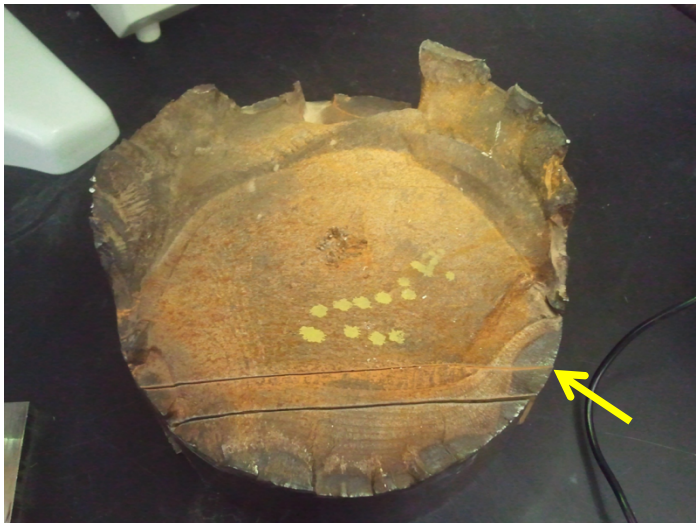

Figure 22: The fracture surface of this 7⍰ mandrel displays all three fatigue fracture stages. The origin of the fracture is identified with an arrow. The fracture then propagated up to the shear lip, which was the last section of the mandrel to fracture.

Figure 23 is an example of a clamshell mark, which is indicative of stage I fatigue. Stage I fatigue is the initiation of a crack and the initial propagation of that crack.

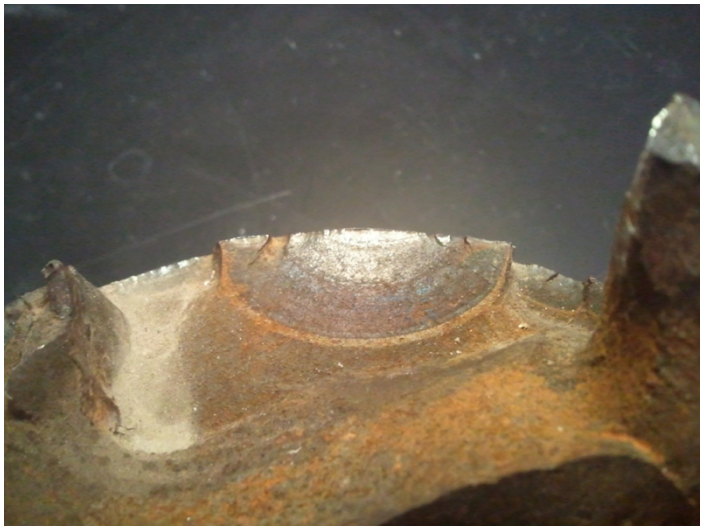

Figure 23: This clamshell mark is from a secondary crack that did not lead to the ultimate failure of the mandrel, but was responsible for degrading the strength of the area of the mandrel that is now the shear lip.

In Figure 24, the initiation sites and clamshell marks are still visible, but are now joined by beach marks with a much larger spacing. These marks are characteristic of stage II fatigue.

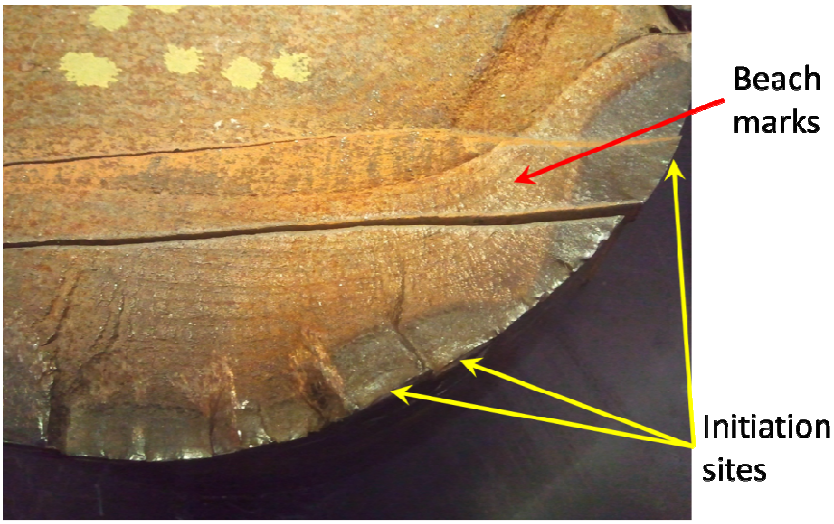

Figure 24: The darker regions at the surface of the mandrel are all initial cracks that eventually joined together to form one large crack front that simultaneously reached the point of stage II fatigue.

Heat Treatments and Charpy Impact Tests

The heat treatments mostly resulted in hardness values within the desired specifications. The exception was with the 600°F tempering treatment. For this heat treatment, despite redoing the heat treatment, the sample had a hardness value of 42.5 HRC instead of the desired 48 HRC. Table III lists the hardness and Charpy impact test energy absorbed for all of the heat treatments conducted.

Table III: Charpy impact energy for quenched and tempered samples.

Tempering Temperature (°F)	Hardness (HRC)	Average Energy Absorbed (ft-lb)	
1202	28.5	82	
		80	
		77	
		Average	79.7
		Std. Dev.	2.52
842	39.8	19	
		16	
		20	
		Average	18.3
		Std. Dev.	2.08
600	42.5	11.5	
		8.5	
		11.5	
		Average	10.5
		Std. Dev.	1.73

The energy absorbed result from the Charpy impact test provides a measure of the quantity of energy that the material is able to absorb before it fractures. The more energy that the material can absorb into and transmit out of its structure, the higher its toughness. For quenched and tempered steel, as the hardness increases, the toughness decreases significantly. At the time of the submission of this paper, austempered samples were being tested for Charpy impact energy, but the results did not arrive in time to incorporate them into the paper.

Discussion

Selecting a new saddling mandrel alloy with a high enough fatigue limit to resist the fatigue associated with the saddling process would be prohibitively expensive; therefore, a different heat treatment for the current mandrel material of 4340 steel is the best option for increasing mandrel lifespan. Hardness is probably the primary material property (that can be easily measured on a batch-to-batch basis) for discerning the fatigue resistance of a mandrel. The harder the material is, the better able it is to resist the initiation and propagation of a crack. Although the stresses reached within the mandrel are unknown, it is probable that the saddling process is a member of low cycle fatigue because of the relatively small amount of cycles until failure (N_f). Low cycle fatigue is defined by low cycles until failure and high stress amplitude.

High toughness will enable the mandrel to absorb much of the impact of the upper die without the localized plastic deformation that leads to the cracks that eventually cause the mandrel to fracture. Table III shows that it is difficult to obtain a combination of high hardness and toughness with quenched and tempered steel. The austempering process results in a material with less residual stresses and a lower dislocation density because the quench to the austempering temperature is less severe than the quench to room temperature for transforming austenite to martensite. The data in Figure 25 is from a study in which the fatigue life of 4340 was analyzed in both the quenched and tempered and austempered conditions. At high stress amplitude, austempered steel shows increased fatigue life.

Most major heat treatment companies are equipped to perform salt bath heat treatments, so any costs above the cost of quench and tempering the mandrels should be minimal. Future study of this problem could include fatigue studies to compare the fatigue life of quenched and tempered and austempered 4340 steel, that information already exists[18]. Because of the uniqueness of fatigue failure under different loading conditions, the most useful data that could be obtained would result from having several mandrels austempered and then testing those mandrels in the actual saddling process. In order to run this test however, a system of logging mandrels and recording the amount of saddling procedures that they have

been used for is essential. This information would provide an estimate for the amount of cycles until failure and could be used to compare mandrels of different heat treatments.

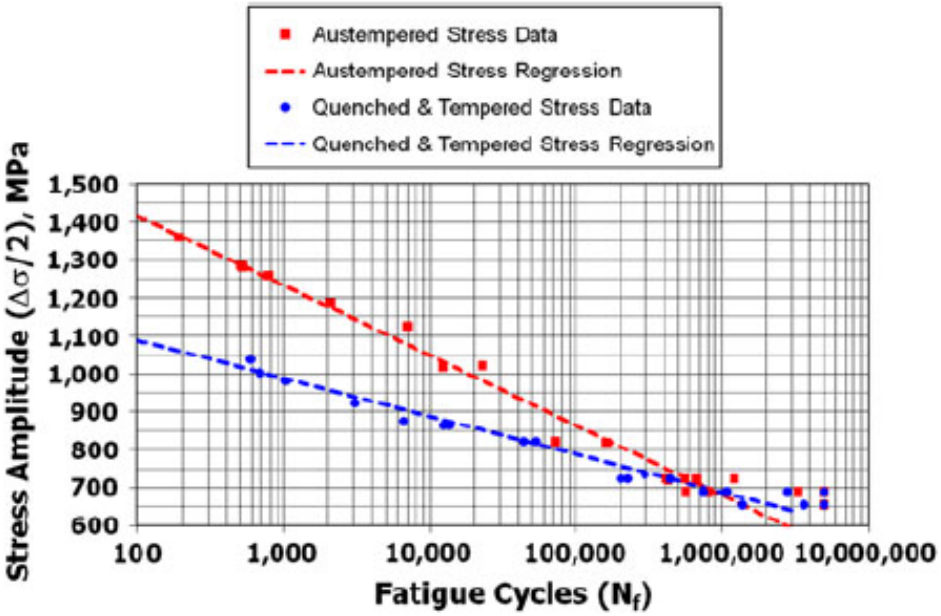

Figure 25: Comparison of fatigue life of Q&T steel and austempered steel based on stress amplitude. High cycle fatigue life seems to be similar for the two treatments, but in the low cycle regime, austempered steel shows a promising increase in fatigue life[18].

Conclusions

1. Saddling mandrels fail by fatigue fracture.
2. Cyclic softening during the saddling process leads to a deterioration of the mechanical properties that inhibit fatigue crack initiation and propagation.
3. An austempering heat treatment may result in increased fatigue life for 4340 steel saddling mandrels.
4. A system of collecting mandrel data is necessary in order to evaluate the effect of changing the saddling mandrel heat treatment on mandrel lifespan.

Acknowledgements

I would like to thank Schlosser Forge Co. for allowing me to work on this project. Nelson Yu (Schlosser Forge) was an exemplary company contact and provided me with answers to all of my questions and helped to set up third party tests in a timely manner. Professor Blair London was an outstanding project advisor, and I attribute much of what I have learned here at Cal Poly San Luis Obispo to him.

References

1. Firth Rixson Limited. Firth Rixson Schlosser. 2012. Online. 1 February 2012. <http://www.firthrixson.com/firth-rixson-schlosser>.

2. Scot Forge. "Forging Solutions: Open Die and Rolled Ring Forging - the Processes, Applications and Benefits." 1998. www.scotforge.com. PDF. 1 February 2012.

3. Granta Design Limited. CES EduPack. 7.0.0.2. Cambridge, 2011. Software.

4. Philip, T.V. and T.J. McCaffrey. "Ultrahigh-Strength Steels, Properties and Selection: Irons, Steels, and High-Performance Alloys." ASM Handbook 1 (1990): 430-448. Online.

5. Massachusetts Institute of Technology. MIT Open Courseware. 2012. Online. February 2012.

6. Meyrick, Glyn and Robert H. Wagoner. "Physical Metallurgy of Steel." 8 January 2001. Document.

7. American Society for Metals. "Atlas of Isothermal Transformation and Continuous Cooling Diagrams." American Society for Metals (1977).

8. Abbaschian, Reza, Lara Abbaschian and Robert E. Reed-Hill. Physical Metallurgy Principles. Fourth. Stamford: Cengage Learning, 2010. Print.

9. Aliya, D. and S. Lampman. "Physical Metallurgy Concepts in Interpretation of Microstructures." ASM Handbook 9 (2004): 44-70. Online.

10. Bramfitt, Bruce L. "Structure/Property Relationships in Irons and Steels." ASM Handbooks (2002). Online.

11. TWI Ltd. "TWI." 2000. Drill pipe failure explained. Online. February 2012.

12. Kerlins, Victor, and Austin Phillips. "Modes of Fracture." *ASM Handbooks Online*. McDonnell Douglas Astronautics Company, 2002. Web. 17 May 2012.

13. ABET Criteria for Accrediting Engineering Programs 2010-13, General Criteria for Baccalaureate Level Programs, General Criteria 3: Student Outcomes (c), www.abet.org/engineering-criteria-2012-2013.

14. Bureau of Labor Statistics. Workplace Injuries and Illnesses - 2010. N.p.: U.S. Department of Labor, 2011. 15. Web. 8 Apr. 2012.

15. ASTM Standard E18-11, 2011, "Standard Test Methods for Rockwell Hardness of Metallic Materials," ASTM International, West Conshohocken, PA, 2012, DOI: 10.1520/E0018-11

16. ASTM Standard E23-07a, 2007, "Standard Test Methods for Notched Bar Impact Testing of Metallic Materials," ASTM International, West Conshohocken, PA, 2007.

17. Landgraf, Ronald W. "Fatigue Resistance and Microstructure of Ferrous Alloys." *ASM Handbooks Online*. ASM International, 2002. Web. 17 May 2012.

18. Tartaglia, John M., and Kathy L. Hayrynen. "A Comparison of Fatigue Properties of Austempered Versus Quenched and Tempered 4340 Steel." *ASM International* 21 June (2012): 1008-24. *Academic Search Elite*. Web. 19 May 2012.